

A Remarkable Difference That One Fluorine Atom Confers on the Mechanisms of Inactivation of Human Ornithine Aminotransferase by Two Cyclohexene Analogues of γ -Aminobutyric Acid

Wei Zhu, Peter F. Doubleday, Daniel S. Catlin, Pathum M. Weerawarna, Arseniy Butrin, Sida Shen, Zdzislaw Wawrzak, Neil L. Kelleher, Dali Liu, and Richard B. Silverman*



Cite This: <https://dx.doi.org/10.1021/jacs.0c00193>



Read Online

ACCESS |



Metrics & More

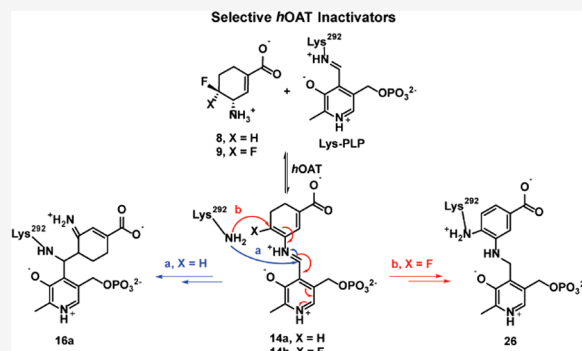


Article Recommendations



Supporting Information

ABSTRACT: Human ornithine aminotransferase (*hOAT*), a pyridoxal 5'-phosphate-dependent enzyme, plays a critical role in the progression of hepatocellular carcinoma (HCC). Pharmacological selective inhibition of *hOAT* has been shown to be a potential therapeutic approach for HCC. Inspired by the discovery of the nonselective aminotransferase inactivator (1*R*,3*S*,4*S*)-3-amino-4-fluoro cyclopentane-1-carboxylic acid (**1**), in this work, we rationally designed, synthesized, and evaluated a novel series of fluorine-substituted cyclohexene analogues, thereby identifying **8** and **9** as novel selective *hOAT* time-dependent inhibitors. Intact protein mass spectrometry and protein crystallography demonstrated **8** and **9** as covalent inhibitors of *hOAT*, which exhibit two distinct inactivation mechanisms resulting from the difference of a single fluorine atom. Interestingly, they share a similar turnover mechanism, according to the mass spectrometry-based analysis of metabolites and fluoride ion release experiments. Molecular dynamics (MD) simulations and electrostatic potential (ESP) charge calculations were conducted, which elucidated the significant influence of the one-fluorine difference on the corresponding intermediates, leading to two totally different inactivation pathways. The novel addition-aromatization inactivation mechanism for **9** contributes to its significantly enhanced potency, along with excellent selectivity over other aminotransferases.



INTRODUCTION

Hepatocellular carcinoma (HCC), which accounts for 90% of primary liver cancer, is the second most common cause of cancer death worldwide.^{1–4} To date, there is no effective treatment for HCC, as it is typically diagnosed at advanced disease stages and tumors are typically refractory to systemic treatment with the standard-of-care receptor tyrosine kinase inhibitor, sorafenib, and radiotherapy.^{5–8} Human ornithine aminotransferase (*hOAT*) is a pyridoxal 5'-phosphate (PLP)-dependent enzyme⁹ with roles in inborn errors of metabolism¹⁰ and hepatocellular carcinoma (HCC) progression.¹¹ Mechanistically, two coupled half-reactions are involved in the transamination cycle of *hOAT* (Figure 1). In the first-half reaction, *hOAT* catalyzes the conversion of PLP and ornithine to pyridoxamine phosphate (PMP) and glutamyl-5-semialdehyde, which spontaneously cyclizes to Δ^1 -pyrroline-5-carboxylate (P5C).¹² The P5C generated can be further converted to proline by pyrroline-5-carboxylate reductase (PYCR).^{13,14} In the second-half reaction, PMP and α -ketoglutarate (α -KG) are converted to PLP and *L*-glutamate (*L*-Glu), which also can be converted to P5C by pyrroline-5-carboxylate synthase (P5CS). Mounting evidence indicates that proline metabolism plays an important role in metabolic

reprogramming to sustain cancer proliferation along with the upregulated synthesis of P5C as a central intermediate.^{15–17} Metabolic reprogramming in HCC is characterized by the activation of the proline/hydroxyproline metabolic pathway, which supports HIF1 α -dependent tumor progression and sorafenib resistance.¹⁸ Furthermore, the glutamate generated by *hOAT* can be converted to glutamine by glutamine synthetase (GS) (Figure 1), which supports anabolic and proliferative cell programs.¹⁹ *hOAT* and glutaminogenic enzymes are found to be strongly activated and commonly overexpressed in HCC because of aberrant, oncogenic Wnt/ β -catenin signaling.^{20,21} The selective inhibition of *hOAT* has been shown to effectively suppress HCC tumor growth *in vivo*.¹¹ More recently, the specific knockdown of *hOAT* was also found to suppress the growth of nonsmall cell lung cancer

Received: January 7, 2020



ACS Publications

© XXXX American Chemical Society

A

<https://dx.doi.org/10.1021/jacs.0c00193>
J. Am. Chem. Soc. XXXX, XXX, XXX–XXX

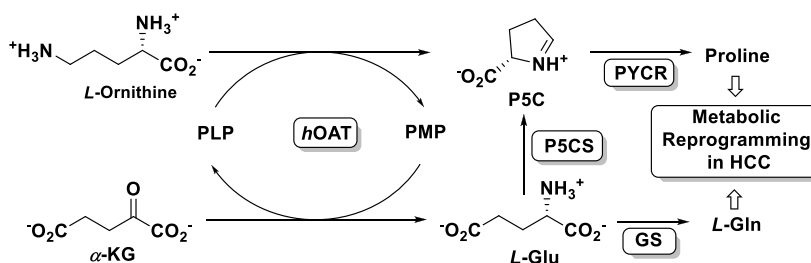
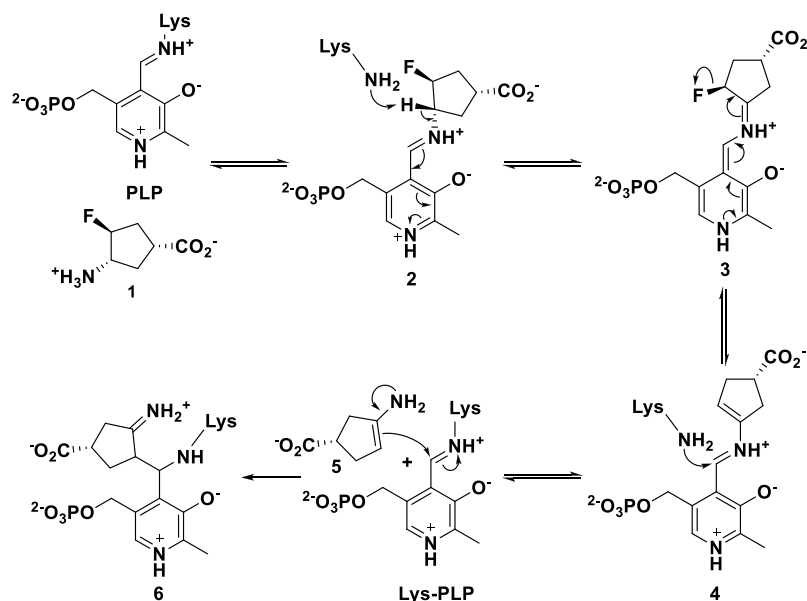


Figure 1. Metabolic pathway for ornithine.

Scheme 1. Mechanism of Inactivation of hOAT and GABA-AT by 1



(NSCLC) *in vitro* and *in vivo*.²² Taken together, hOAT plays an important role in the metabolic reprogramming of HCC via proline and glutamine metabolic pathways, and the selective inhibition of hOAT serves as a promising therapeutic strategy for the treatment of HCC and other related cancers.

Among 14 known aminotransferases, hOAT belongs to the same subgroup as γ -aminobutyric acid aminotransferase (GABA-AT) because of their similarities in primary structures.²³ hOAT and GABA-AT have very similar active sites,²⁴ so it is not surprising that some potent inhibitors of GABA-AT also inhibit hOAT.¹¹ Over many years, our laboratory has been focusing on the rational design of mechanism-based inactivators (MBIs) of GABA-AT.²⁵ MBIs are unreactive alternate substrates for target enzymes, which are converted to active species in the catalytic site and then lead to inactivation via covalent bonding with the enzyme, tight-binding inhibition, or any functionally irreversible inhibition mechanism.²⁶ For example, (1R,3S,4S)-3-amino-4-fluorocyclopentane-1-carboxylic acid (1) was reported to inactivate hOAT²⁷ and GABA-AT²⁸ via the same enamine mechanism, as shown in Scheme 1. The proposed inactivation mechanism is initiated by the formation of Schiff base 2, which is subjected to rate-determining deprotonation and *in situ* elimination of fluoride ion to afford intermediate 4. Active enamine 5 is formed via a Schiff base exchange reaction, and the subsequent nucleophilic addition of 5 to the Lys-bound PLP complex yields covalent adduct 6.

Because MBIs are inert until they are activated in the active site, undesirable off-target effects can be greatly reduced. More importantly, these inactivators can demonstrate higher potency and selectivity than traditional inhibitors even at a lower dosage.^{11,29,30} In 2015, GABA analogue 7 (Figure 2) was

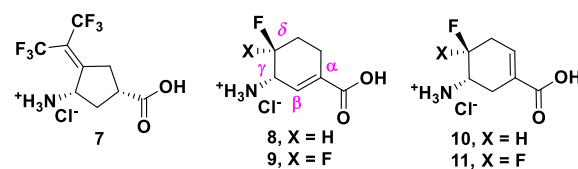
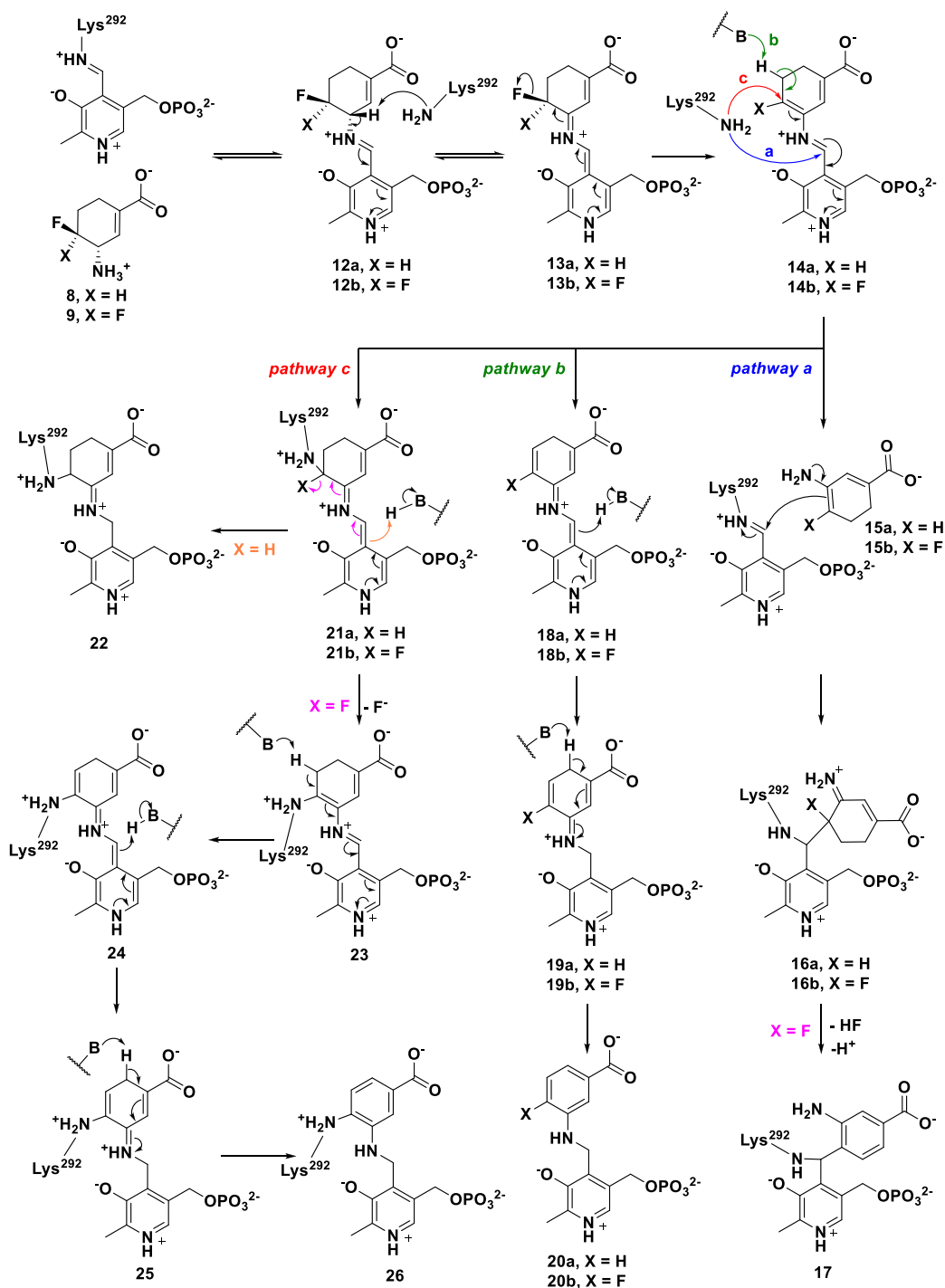


Figure 2. Structures of selective hOAT inactivators 7 and fluorine-substituted cyclohexene analogues 8–11.

reported as a selective MBI of hOAT, which dramatically reduced α -fetoprotein levels (a biomarker for HCC) and suppressed *in vivo* HCC tumor growth at doses of 0.1 and 1.0 mg/kg.¹¹ Very recently, the inactivation mechanism of 7 was also revealed.³¹

We have been interested in discovering potent and selective hOAT inactivators that have novel inactivation mechanisms. Herein, we rationally designed and synthesized fluorine-substituted cyclohexene-based GABA analogues 8–11 (Figure 2) based on the cyclopentane-based analogue 1. Among them, compound (9) is 23 times more efficient as an inactivator of hOAT than 7, along with excellent selectivity over other aminotransferases (e.g., GABA-AT). We also elucidated the

Scheme 2. Possible Inactivation Mechanisms for 8 and 9

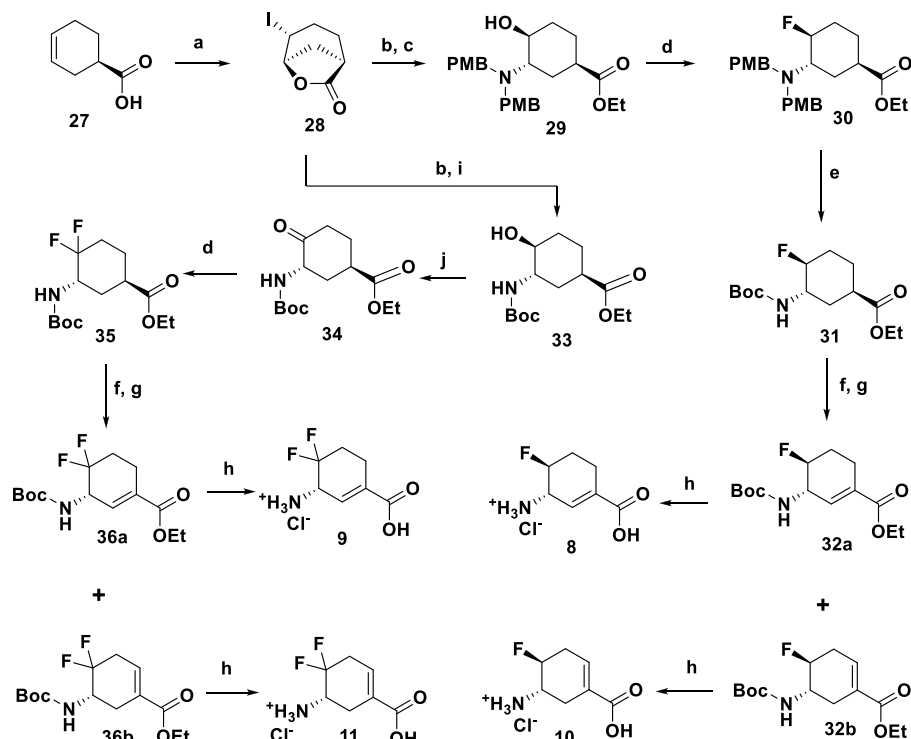


inactivation and turnover mechanisms for 8 and 9 through mass spectrometry, crystallography, and various other biochemical methods and can conclude that a difference of a single fluorine atom dramatically alters the inactivation mechanism.

RESULTS AND DISCUSSION

Design of Novel OAT Inactivators. Similar binding pockets are observed in *hOAT* and GABA-AT, which produce virtually identical distances between the anchor points of the ligands. Interestingly, Tyr55 in *hOAT* partially occupies a similar steric space as does Phe351 in GABA-AT. The more

hydrophobic Phe351 residue intrudes into the active site of GABA-AT so that only the smaller GABA molecule can fit; the *hOAT* catalytic site is more flexible and larger to accommodate ornithine that is one carbon longer than GABA.³² Furthermore, the unique Tyr55 residue provides the potential of forming extra hydrogen bonds with the more hydrophilic substrate in the active site of *hOAT*.³¹ Previously, cyclopentane-based GABA analogue 1 was identified as a dual inhibitor against *hOAT* and GABA-AT. Because of the relatively small size of 1, it can fit into the catalytic pockets of *hOAT* and GABA-AT, consistent with its poor selectivity.²⁷ Thus, we hypothesized that the relatively larger sizes of

Scheme 3. Syntheses of Fluorine-Substituted Cyclohexene Derivatives 8–11^a

^aConditions: (a) NaHCO₃, I₂, KI, H₂O, 0 °C to r.t., overnight; (b) NaOH, EtOH, 0 °C to r.t., 3 h; then ammonia solution (28–30%), EtOH, 45 °C, overnight; (c) 4-anisaldehyde, AcOH, NaBH(OAc)₃, DCE, 75 °C, overnight; (d) XtalFluor-M, (HF)₃Et₃N, DCM, in a plastic container, r.t., overnight; (e) Pd(OH)₂, Boc₂O, MeOH, EtOAc, r.t., overnight; (f) PhSeCl, KHMDS (1 M in THF), –78 °C; (g) *m*-CPBA, DCM, r.t., 2 h; (h) HCl (4M), AcOH, 80 °C, overnight; (i) Boc₂O, EtOH, 0 °C to r.t., 5 h; (j) PCC, DCM, r.t., overnight.

cyclohexene derivatives 8–11 could potentially improve their *h*OAT selectivity over GABA-AT (Figure 2). In addition, the incorporation of a double bond at the α/β -position (8/9) could possibly enhance the inhibitory activity³³ compared with the double bond isomers 10/11, potentially by increasing the acidity of the proton adjacent to the amino group.

MBIs usually act as substrates initially, followed by the formation of active intermediates at the catalytic site, which then inactivate the enzymes through different mechanistic pathways. Therefore, a proposal of the inactivation mechanism plays an important role in the early stage of rational design of potential MBIs. Three possible inactivation mechanisms for 8/9 are proposed in Scheme 2. All of the mechanisms are initiated by Schiff base formation (12a/12b) with subsequent HF elimination to give reactive species 14a/14b, based on the known mechanism of 1 (Scheme 1). Mechanistic pathway *a* is similar to the inactivation mechanism of 1, in which active enamine 15a/15b could be released after transimination of 14a/14b with Lys292. The subsequent enamine addition could lead to inactivation with the formation of adducts 16a/16b. The second fluoride ion of adduct 16b could be further released to afford aromatic adduct 17. Mechanistic pathway *b* is a direct aromatization of 14a/14b to yield a tight binding adduct 20a/20b, which is similar to the inactivation mechanism of another fluorinated cyclohexene analogue.³⁴ Mechanistic pathway *c* involves nucleophilic addition of Lys292 to conjugated olefin 14a/14b, yielding adducts 21a/21b.

In the case of 21b, it is possible to form a more stable covalent aromatic adduct (26) after the elimination of the second fluoride ion.

Molecular Docking. To better understand the difference in steric hindrance between ring sizes, molecular docking studies³⁵ for 1 and 8 were employed to mimic their binding poses at the active sites of GABA-AT and *h*OAT, compared with the native substrates. As shown in Figure S1A, GABA binds in the active site of GABA-AT and establishes hydrogen bonds with residues Arg192, Tyr69, and Glu270. This putative binding pose of GABA positions its γ -amino group close to the Lys329-PLP complex and facilitates the subsequent Schiff base exchange. The binding model of 1 demonstrates similar hydrogen bonds with these residues (Figure S1B). However, molecular docking shows 8 forms a more stable hydrogen bond with His206 to avoid the potential clash with residue Phe351 (Figure S1C), which potentially impedes its initial reaction with Lys329-PLP complex. Comparably, the binding model of ornithine with *h*OAT shows the δ -amino group goes deep into the active site and forms a distinct hydrogen bond with Thr322 (Figure S1D), which positions it close to the Lys292-PLP complex. The amino group of 8 forms a similar hydrogen bond with Thr322 in the docking model (Figure S1E), while the docking pose of 1 indicates it forms a hydrogen bond with Glu325 instead (Figure S1F). These docking results indicate that the larger cyclohexene analogues as substrates are favored in the *h*OAT active site but disfavored in the GABA-AT active site when compared with 1, which matches our design strategy described above.

The chirality of the γ -position of MBIs was found to be very important for the inactivation process and for retaining their inhibitory activity.²⁵ Interestingly, the enantiomer of 8 shows a similar binding pose in the active site of *h*OAT (Figure S1G). Lys-assisted deprotonation at the γ -position proved to be the

Table 1. Kinetic Constants for the Inactivation of *h*OAT and GABA-AT by 1, 7-11, and (S)-Vigabatrin^a

Compound	<i>h</i> OAT			GABA-AT		
	<i>K</i> _i (mM)	<i>k</i> _{inact} (min ^{−1})	<i>k</i> _{inact} / <i>K</i> _i (mM ^{−1} min ^{−1})	<i>K</i> _i (mM)	<i>k</i> _{inact} (min ^{−1})	<i>k</i> _{inact} / <i>K</i> _i (mM ^{−1} min ^{−1})
8	0.031 ± 0.007	0.080 ± 0.007	2.56	2.53 ± 0.71	0.098 ± 0.011	0.039
9	0.0023 ± 0.0007	0.048 ± 0.004	20.33	>0.12 ^b	>0.18 ^b	1.52 ± 0.09 ^b
10	4.38 ± 0.86	0.075 ± 0.005	0.017	1.1 ± 0.14 ^c	0.20 ± 0.001 ^c	0.18 ^c
11	0.54 ± 0.017	0.083 ± 0.013	0.15	4.28 ± 2.05	0.028 ± 0.005	0.0065
1	1.40 ± 0.041	0.086 ± 0.01	0.06	>9.63 ^b	>0.29 ^b	0.030 ± 0.001 ^b
7	0.065 ± 0.010	0.057 ± 0.003	0.87	0.078 ± 0.04	0.017 ± 0.002	0.22
(S)-vigabatrin				0.29 ± 0.09	0.21 ± 0.03	0.72
				3.2 ^{c,d}	0.37 ^{c,d}	0.11 ^{c,d}

^a*k*_{inact} and *K*_i values were determined by the equation: $k_{\text{obs}} = k_{\text{inact}} \cdot [\text{I}] / (K_i + [\text{I}])$ and are presented as means and standard errors. ^bRatio of *k*_{inact}/*K*_i was determined by the slope of $k_{\text{obs}} = k_{\text{inact}} \cdot [\text{I}] / (K_i + [\text{I}])$. *k*_{inact} is greater than maximum *k*_{obs}, which was determined in a time-dependent assay; *K*_i is greater than *k*_{obs}(max)/ratio. ^cAssays tested at pH 6.5. ^dReference 40.

Table 2. Mass Differences of Proposed Adducts between Experimental and Theoretical Mass Values of Native/Modified *h*OAT

Cmpd.	Mechanistic pathways	Adducts	Theoretical mass difference	Experimental mass of native <i>h</i> OAT ^a	Experimental mass of modified <i>h</i> OAT ^a	Experimental mass difference
8	a	16a	369.08	46136.79 ± 0.27	46506.08 ± 0.21	369.29
	b	20a	0			
	c	22	368.06 or 138.03			
9	a	16b	387.05	46138.32 ± 0.10	46504.66 ± 0.13	366.34
		17	366.06			
	b	20b	0			
	c	26	366.06			

^aValues are presented as means and standard errors.

rate-determining step in earlier analogues.³⁶ Thus, the molecule docking study was also conducted to predict the binding poses of active intermediates 12a (Figure S1H) and its enantiomer (Figure S1I) at the catalytic pocket of *h*OAT. Both carboxylate moieties of these intermediates establish hydrogen bonds with Tyr55 and Arg180, while the different chirality of the 12a-enantiomer forces its γ-proton to face the other side, which points away from the catalytic Lys292 (3.0 Å vs 5.3 Å). This docking simulation is also consistent with the observation of earlier inactivators and supports the synthesis of chirally pure analogues.

Syntheses of Fluorine-Substituted Cyclohexene Analogues 8–11. The synthetic route for 8–11 is shown in Scheme 3. The di-PMB intermediate (29) was afforded from chirally pure starting material 27 by three sequential steps: intramolecular annulation, stereoselective epoxide ring-opening, and reductive amination with excess anisaldehyde. The obtained intermediate (29) was treated with XtalFluor-M and (HF)₃Et₃N to exclusively yield trans-isomer 30 in moderate yields in which an aziridinium mechanism pathway might be involved.³⁷ The direct conversion from di-PMB protected intermediate 30 to Boc-protected intermediate 31 was achieved by Pd(OH)₂ catalyzed hydrogenation in the presence of Boc₂O. Intermediate 31 was treated with PhSeCl and KHMDS, followed by oxidative elimination with m-CPBA to yield olefin isomers 32a and 32b, which were separated by chromatography and then deprotected to 8 and 10, respectively. On the basis of a previous report, alcohol 33³⁸ can be prepared from chirally pure 27; 33 was then oxidized by PCC to give ketone 34. After screening various fluorination reagents and reaction temperatures, key intermediate 35 was afforded in moderate yields, which avoided the production of monofluoroalkene impurities.³⁹ Using the same method used

to make 8 and 10, intermediate 35 was converted to difluoroolefin isomers 36a and 36b, which were further deprotected to 9 and 11, respectively.

Kinetic Studies of Fluorine-Substituted Cyclohexene Analogues. *In vitro* studies showed that fluorine-substituted cyclohexene analogues 8–11 inhibited *h*OAT with good selectivity over GABA-AT (Table 1). The results show that the six-membered ring analogues have a lower binding affinity to GABA-AT than 1 with much greater *K*_i values, indicating that the larger ring size potentially interferes with binding interactions between the analogues and GABA-AT, which has a relatively small and rigid active site. The selectivity is consistent with our initial design strategy and docking results for the initial binding step (Figure S1A–F).

The introduction of a double bond at the α/β-position or another fluorine at the δ-position significantly enhances the inactivation efficiency against both *h*OAT and GABA-AT, which could possibly result from the reduced acidity of the γ-position or the change in inactivation mechanisms. Among them, the best compound (9, *k*_{inact}/*K*_i = 20.33 min^{−1}mM^{−1}) is 23 times more efficient as an inactivator of *h*OAT than 7 (*k*_{inact}/*K*_i = 0.87 min^{−1}mM^{−1}), which exhibited potent *in vivo* antitumor efficacy.¹¹ Moreover, 9 displayed good selectivity over GABA-AT with lower efficiency constants (pH 8.0, *k*_{inact}/*K*_i = 1.52 min^{−1}mM^{−1}; pH 6.5, *k*_{inact}/*K*_i = 0.18 min^{−1}mM^{−1}) and little or no inhibitory activities against aspartate aminotransferase (Asp-AT) and alanine aminotransferase (Ala-AT), even at high concentrations (5–20 mM, Figure S2).

Inactivation mechanisms of 8 and 9 were studied for a better understanding of the capabilities of the aminotransferase and for future rational design of new inactivators. To determine if any of the aforementioned mechanisms (Scheme 2) are responsible for the inactivation of *h*OAT by 8 and 9, we carried

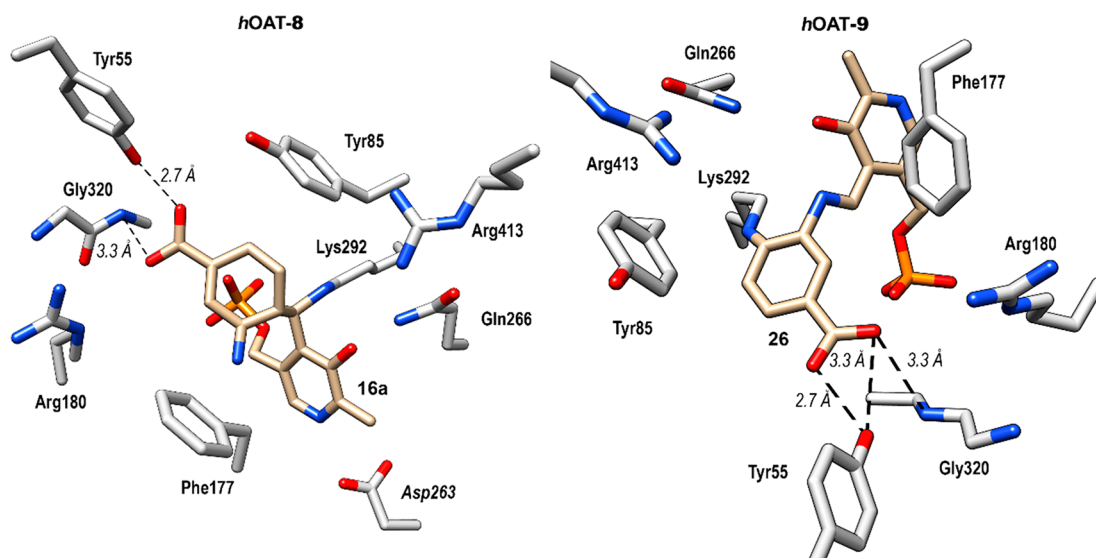


Figure 3. Co-crystal structures of *hOAT* inactivated by **8** (left) and **9** (right).

out a series of experiments, including dialysis and fluoride ion release studies, and obtained protein mass spectra and crystal structures of the inactivated enzymes.

Dialysis. Although **8** and **9** were designed to inactivate *hOAT* via a covalent or tight-binding mechanism, time-dependent reactivation of *hOAT* was carried out to determine if reversible components were also involved during the inactivation.³⁰ After *hOAT* activity was partially or fully abolished by 4–25 equiv of **8** or 0.6–2.0 equiv of **9**, they were dialyzed, and aliquots at different time intervals were collected and assayed for return of enzyme activity. No enzyme activity was recovered after 48 h of dialysis (Figure S3), indicating complete irreversible inhibition of *hOAT*.

Intact Protein Mass Spectrometry of *hOAT* Modified by **8 or **9**.** Intact protein mass spectrometry has served as an efficient tool to determine the covalent adducts or tight binding adducts of modified aminotransferases.^{31,41} Notably, the hydrolysis of imine groups and loss of PLP or PMP were commonly observed.³¹ With the existing unstable groups in native *hOAT* or potential covalent adducts being taken into account, the theoretical mass differences were calculated as shown in Table 2. When *hOAT* was inactivated by **8**, one modified species (46506.08 ± 0.21 Da) was observed by mass spectrometry. A mass shift of +369.29 Da was observed, which corresponds to adduct **16a** in pathway *a* (Scheme 2). In the case of **9**, a mass shift of +366.34 Da was observed from the native enzyme (46138.32 ± 0.10 Da) and one modified species (46504.66 ± 0.13 Da) detected by mass spectrometry. This mass shift corresponds to either adduct **17** in pathway *a* or adduct **26** in pathway *c* (Scheme 2).

X-ray Crystallography of *hOAT* Inactivated by **8 or **9**.** Although a highly accurate mass shift of +369.29 Da was observed in the intact protein mass spectrum of *hOAT* inactivated by **8**, there is only a 1.02 Da difference between adducts **16a** and **22**. In addition, it is difficult to distinguish adducts **17** and **26** by intact protein mass spectrometry of inactivated *hOAT* by **9**. To better interpret the inactivation mechanism(s) for **8/9**, protein crystallography of *hOAT* inactivated by **8/9** was conducted to confirm the adducts formed in the active site, respectively.

The structure of *hOAT* inactivated by **8/9** was solved by molecular replacement using a monomer from a previously reported structure of *hOAT* (PDB code 1OAT), after all water molecules and ligand atoms were deleted. For *hOAT-8*, in space group C121, one asymmetric unit was found to contain 3 monomers. Two monomers in the asymmetric unit formed a biological assembly as a homodimer. The third monomer formed a homodimer with another monomer present in another asymmetric unit. For *hOAT-9*, in space group *P*₃12, one asymmetric unit was also found to contain 3 monomers. The biological assemblies can be observed through crystallographic symmetry. Final models for *hOAT-8* and *hOAT-9* were refined to a resolution of 2.20 and 1.90 Å, with *R*_{Free}/*R*_{work} values of 15.70%/19.90% and 27.49%/23.98%, respectively. Final refinement statistics are presented in Table S1. A polder map⁴² for each structure was generated by omitting PLP, ligand, and Lys292 (Figure S4). The density for PLP was clearly represented in the polder map for both structures. Densities for **8** and **9** were also observed, clearly showing the presence of a ring and carboxylate moiety, as expected for the final adducts. The solved structures of *hOAT-8/9* have been deposited in the PDB bank (PDB codes: 6V8D and 6V8C).

Ternary adducts were observed within both active sites of *hOAT-8* and *hOAT-9*. As seen in Figure S5, **8** and **9** reacted with and covalently linked to both PLP and Lys292, albeit at different positions, each forming ternary adducts. In the *hOAT-8* crystal structure, PLP and Lys292 are linked with the inactivator at a central carbon atom, affording **16a**. This result agrees with the MS data and rules out **22** as the final adduct, where PLP and Lys292 form covalent bonds at different positions with the inactivator. Therefore, pathway *a* is the most probable mechanism of inactivation by **8**, rather than pathway *c* (Scheme 2). In the *hOAT-9* crystal structure, Lys292 and PLP form covalent bonds with the inactivator to give **26**. No density was observed to suggest a fluorine atom remained on the adduct. The complete loss of fluorine and the presence of covalent bonds on the adduct thereby excludes pathway *b* (Scheme 2) as a possible mechanism for inactivation, as was concluded by intact protein mass spectrometry. The ternary adduct in the active site of *hOAT-9* is linked at two separate positions along the ring, rather than at a central atom as in **17**.

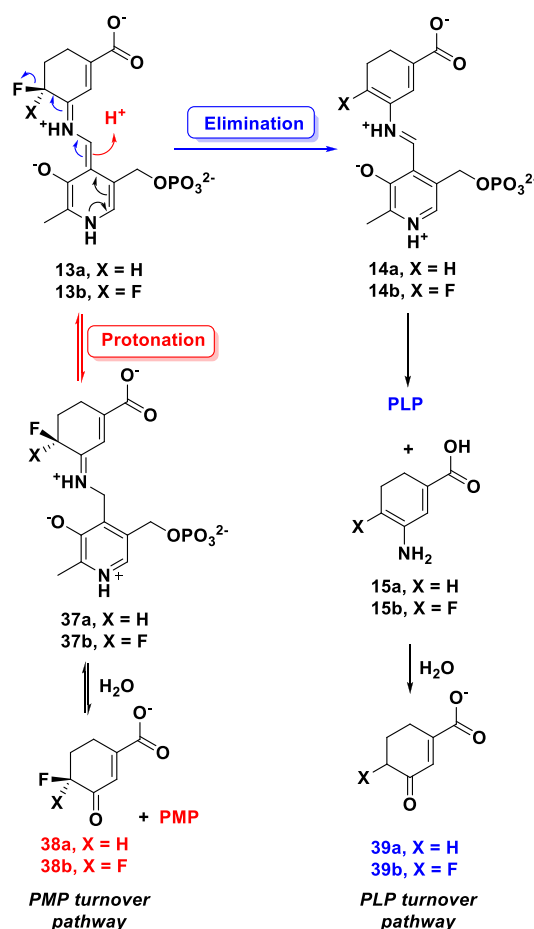
The electron density generated by the polder map ($F_o - F_c$) completely encloses the C–N bond formed between the lysine and PLP, suggesting **9** inactivates *hOAT* via pathway *c* to **26** (Scheme 2). Furthermore, Thr322 is positioned at the center of the six-membered ring and appears to form a lone-pair–aromatic interaction⁴³ (2.9 Å) with the adduct (Figure S5), which supports the formation of **26**.

As shown in Figure 3 (right), both oxygen atoms on the carboxylate of **26** establish hydrogen bonds with Tyr55 (2.7 and 3.3 Å), whereas only one oxygen atom on the carboxylate of **16a** (Figure 3, left) was observed to engage in a hydrogen bond with Tyr55 (2.7 Å). The interaction with Tyr55 has precedence; there is a similar interaction in the crystal structure of inactivated *hOAT*-7.³¹ The carboxylates of both **16a** and **26** were observed to form an $n-\pi^*$ interaction with the peptide backbone of Gly320 (both 3.3 Å) but no interaction with Arg180, which is essential for native substrate recognition.⁴³ Tyr55 is a unique residue in the active site of *hOAT*, compared with that of GABA-AT, which is assumed to form a hydrogen bond with the α -amino group of ornithine.^{44,45} The interaction of GABA analogues **8** and **9** with Tyr55 contributes to their high potency, even though they are one carbon less than the native substrate ornithine.

Turnover Mechanism. Previously, it was found that **1** can be converted to metabolites by aminotransferases, with the release of PLP or PMP.²⁷ Considering the structural similarity between **1** and **8/9**, two possible turnover pathways are proposed, as shown in Scheme 4. Schiff base formation of PLP with **8/9** and subsequent lysine-assisted deprotonation yields intermediates **13a/13b**. Intermediates **13a/13b** could be converted to intermediates **37a/37b** via direct protonation of the coenzyme. The formed imines could be further hydrolyzed with the release of PMP and metabolites **38a/38b**. This PMP turnover mechanism is similar to the degradation of ornithine by *hOAT*. Intermediates **13a/13b** also could undergo elimination of fluoride ion and hydrolysis of the imine with release of enamines **15a/15b**, which could be hydrolyzed to afford ketones **39a/39b**. In this PLP turnover mechanism, the regenerated PLP would further form Schiff bases with inactivators even in the absence of α -KG. To determine if any of the above turnover mechanisms are involved during the inactivation process of *hOAT* by **8** and **9**, we carried out a partition ratio experiment, determination of fluoride ion release, and mass spectrometric analysis of metabolites for these two inactivators.

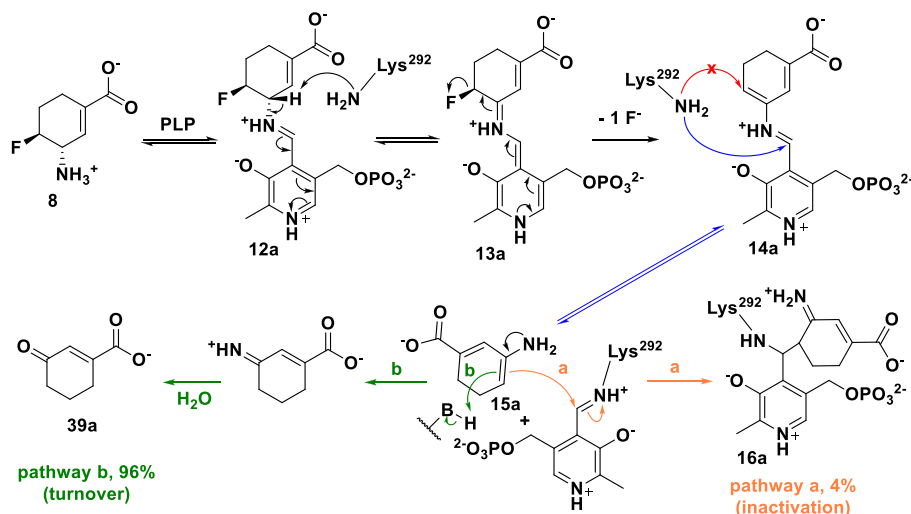
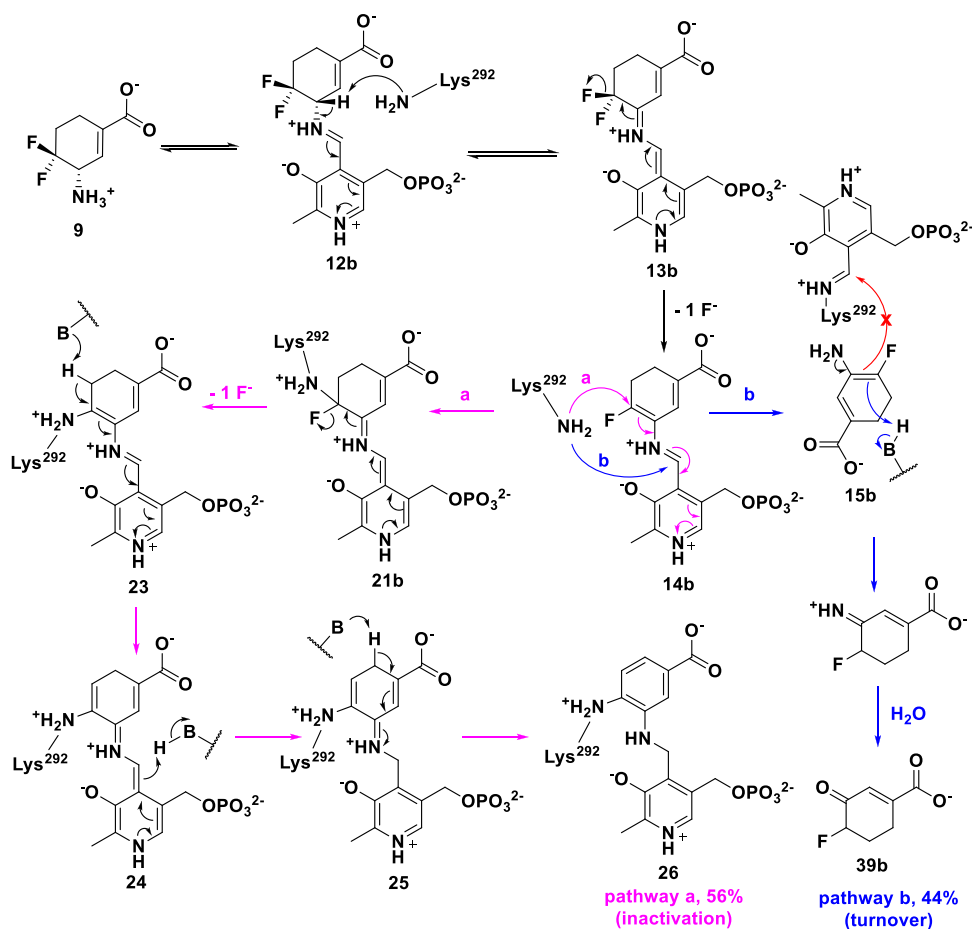
Partition Ratio and Fluoride Release. The partition ratio is the ratio of the compound acting as a substrate relative to the compound inactivating the enzyme. Ideally, a plot of enzyme activity remaining vs equivalents of compounds added will give a straight line from 100 to 0% enzyme activity remaining. The intercept with the x -axis gives the number of inactivator molecules required to inactivate each enzyme molecule (the turnover number). This number includes the one molecule of inactivator required to inactivate the enzyme; consequently, the partition ratio is the turnover number minus one (assuming there is a 1:1 stoichiometry of inactivator to enzyme). Therefore, the partition ratios of **8/9** were determined by titrating the enzyme with varying equivalents of inactivator with a known amount of *hOAT* (Figure S6). The linear relationship was extrapolated to yield the exact equivalents required to inactivate the enzyme completely. From this, we determined the partition ratio of **8** to be 22.0 and the partition ratio of **9** to be 0.8.

Scheme 4. Proposed Turnover Mechanism for **8** or **9** by *hOAT*



Different equivalents of fluoride ions can be released in PLP and PMP turnover pathways.^{29,31} In the absence of α -KG, if PMP is formed in the turnover mechanism, it cannot be converted back to PLP, which results in less than one equivalent of fluoride ion released. If PLP is regenerated during the turnover mechanism after fluoride ion is released, multiple equivalents of fluoride ions will be released. The number of fluoride ions released per enzyme turnover can be detected using a fluoride ion selective electrode. When *hOAT* is inactivated with an excess of **8** in the absence of α -KG, 22.7 equiv of fluoride ions were released per enzyme active site (Table S2). In the case of **9**, 2.9 equiv of fluoride ions were released per enzyme active site (Table S2). These results indicate that turnover mechanisms of **8** and **9** must regenerate PLP as part of the turnover mechanism with the release of additional equivalents of fluoride ion before inactivation, which is consistent with their partition ratios, respectively.

Mass Spectrometry-Based Analysis of Metabolites. After size exclusion filtration of inactivated *hOAT* samples **8/9**, the filtrate was analyzed by untargeted metabolomics (\pm ESI HRMS) to detect metabolites. As shown in Figure S7, metabolites **39a** (m/z 139.0393, $[M-H]^{-1}$) and **39b** (m/z 157.0301, $[M-H]^{-1}$) in the PLP turnover pathway were detected and confirmed by their fragmentation spectra. Standards of PLP and PMP were monitored by HRMS, and the HCD-based fragmentation of precursors was used to confirm metabolite detection and retention time (Figure S8A,B). In both samples of **8** and **9**, only PLP was detected

Scheme 5. Plausible Mechanism for 8 with *h*OATScheme 6. Plausible Mechanism for 9 with *h*OAT

by mass spectrometry (m/z 248.0316, $[M + H]^+$); neither PMP nor adducts of PMP were observed (Figure S8C,D). Overall, metabolomic results indicate these two compounds undergo a similar PLP regeneration turnover mechanism (Scheme 4).

Plausible Mechanisms for 8 and 9 with *h*OAT. On the basis of the above inactivation and turnover mechanism studies, a modified mechanism pathway for inactivator 8 is shown in Scheme 5. Schiff base 12a is initially formed and

subsequently deprotonated to afford intermediate 13a. On the basis of the fluoride ion release experiment and the metabolomics results, intermediate 13a is fully converted to intermediate 14a. Schiff base 14a is then attacked by Lys 292 at the PLP imine position instead of the conjugate olefin position. According to the partition ratio of 8, only 4% of active enamine 15a attacks the Lys-PLP complex for inactivation (pathway a), and 96% of that is hydrolyzed to yield 39a (pathway b).

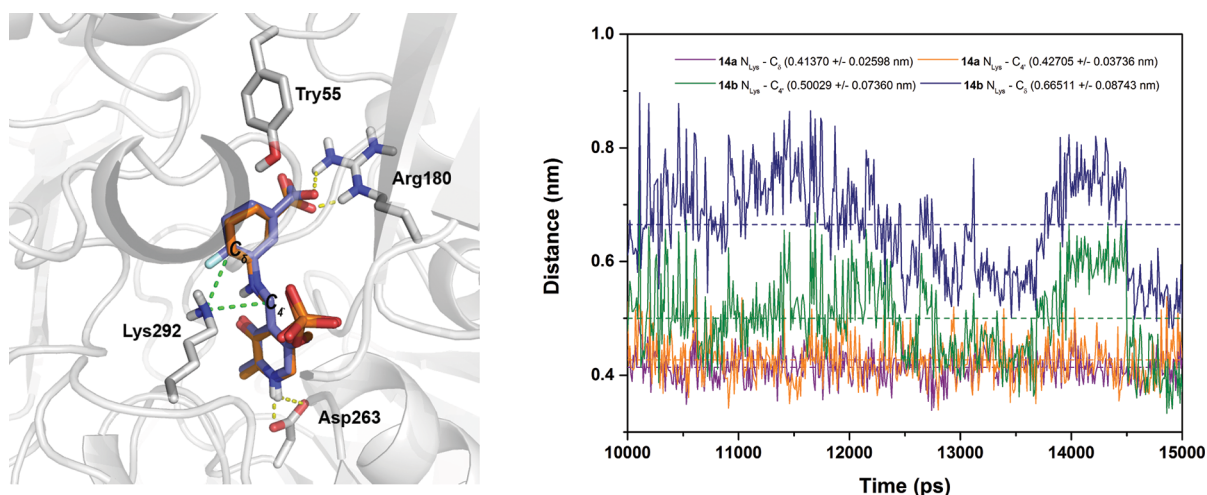


Figure 4. Molecular docking of **14a** (orange) and **14b** (blue) in the active site of *hOAT* (left); distance changes between N_{Lys} and C_δ / $C_{4'}$ of **14a** and **14b** during molecular dynamics (right).

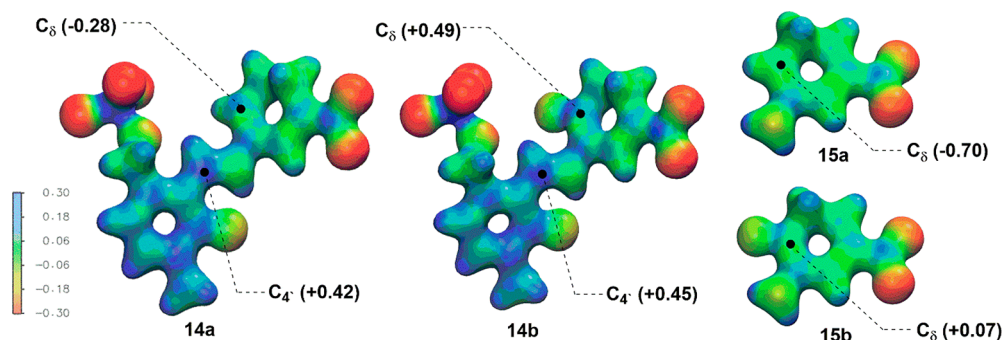


Figure 5. Electron density maps colored coded to the electrostatic potential of intermediates and ESP charges of C_δ and $C_{4'}$.

As shown in in [Scheme 6](#), a modified mechanism pathway for inactivator **9** is proposed. Although active intermediate **14b** is formed via a similar fluoride ion release process, inactivation occurs by lysine addition at the conjugated double bond. The formed adduct is further converted to the more stable aromatic adduct (**26**; 56%, *pathway a*), and 44% of intermediate **14b** is converted to inert enamine **15b**, which does not attack the Lys-PLP complex, and is hydrolyzed to yield metabolite **39b** instead (*pathway b*).

The structure of adduct **16a/26** was confirmed by intact protein MS and its crystal structure complex, and the corresponding metabolite **39a/39b** was detected by mass spectrometry, along with multiple equivalents of fluoride ion released. Taken together, the difference of a single fluoride atom results in different inactivation mechanism pathways for **8** (*enamine pathway*) and **9** (*addition-aromatization pathway*) but by the same turnover mechanism (*PLP pathway*).

Molecular Dynamics (MD) Simulations and Electrostatic Potential (ESP) Charge Calculations. Although very similar intermediates (**14a/14b** and **15a/15b**) are formed during inactivation by **8** and **9**, the resulting covalent adducts (**16a** and **26**, respectively) are quite different. Previously, different inactivation mechanisms for alanine racemase inhibitors were demonstrated as a result of a different number of fluorines (one-fluorine vs three-fluorines).⁴⁶ For a better understanding of the impact the additional fluoride atom had on these intermediates, molecular docking/dynamics and ESP charge calculations were carried out to demonstrate their

binding poses in the catalytic pocket of *hOAT* and reaction affinity with Lys292 or the Lys292-PLP complex.

As shown in [Figure 4A](#), the docking poses of **14a** and **14b** are almost identical in the active site of *hOAT*, where Lys292 lies in the middle of two potential electrophilic sites: the carbon of the PLP imine moiety ($C_{4'}$) and the terminal carbon of the conjugated olefin (C_δ). Molecular dynamics simulations were conducted to calculate the average distance between the nitrogen of the nucleophilic Lys292 (N_{Lys}) and the $C_{4'}$ / C_δ positions of **14a/14b**, respectively ([Figure 4B](#)). The average distance of $N_{Lys}-C_{4'}$ (4.3 Å) and $N_{Lys}-C_\delta$ (4.1 Å) in **14a** is very similar, whereas the $C_{4'}$ of **14b** is closer to the N_{Lys} (5.0 Å) than the C_δ of **14b** (6.6 Å), with an average difference of 1.6 Å. The average dihedral angles between the cyclohexadiene rings and the pyridine rings were also monitored during the molecular dynamics simulations ([Figure S9](#)). The average dihedral angle of **14b** (-148.26°) is much closer to -180° (fully conjugated) than that of **14a** (-91.64° ; orthogonal and not in conjugation), indicating that the olefin in **14b** has a greater propensity to conjugate with the pyridine ring. ESP charges ([Figure S10](#)) and electron density/electrostatic potential maps ([Figure 5](#)) for intermediates **14a/b** and **15a/b** were calculated to evaluate the impact of the additional fluoride atom. The significant differences are demonstrated between C_δ -**14a** (-0.28) and C_δ -**14b** ($+0.49$) with the introduction of an additional fluoride atom, as well as C_δ -**15a** (-0.70) and C_δ -**15b** ($+0.07$), while the charge at $C_{4'}$ -**14a** ($+0.42$) is close to that at $C_{4'}$ -**14b** ($+0.45$). Therefore, from the molecular dynamics simulation ([Figure 4](#)) the accessibility of

Lys292 to C₈-**14a** and C₄'-**14a** is similar, but the dihedral angle (−91.64°) and carbon charges (−0.28 vs +0.42) significantly disfavor nucleophilic attack of Lys292 on the olefin of **14a**; attack at C₄' gives enamine **15a** and leads to final adduct **16a** (Scheme 5). In the case of **14b**, the distance N_{Lys}-C₄' is favored for nucleophilic attack of Lys at C₄' of **14b** relative to C₈ of **14b** (5.0 Å vs 6.6 Å), but the electrophilicity of the C₈ of **14b** is greatly enhanced by the additional fluorine atom, resulting in the generation of final adduct **26** and inactive enamine **15b**, which gets protonated and hydrolyzed to **39b** (Scheme 6). The additional fluorine atom in **15b** significantly decreases its nucleophilicity, which prevents the formation of adducts **16b** and **17** (Scheme 2). Both molecular docking/dynamics and ESP charge calculations clearly rationalize our observations during the inactivation of hOAT by **8** and **9**.

CONCLUSIONS

Over the past few years, selective inhibition of human ornithine aminotransferase (hOAT) has been gradually recognized as a potential treatment for cancers, especially hepatocellular carcinoma (HCC).¹¹ On the basis of the known inactivation mechanism for nonselective inactivator **1**,³¹ a novel class of fluorine-substituted cyclohexene analogues (**8**–**11**) was rationally designed, with the aid of molecular dynamics simulations and docking, synthesized, and evaluated. Among them, analogues **8** and **9** showed significantly improved inhibitory activities against hOAT with excellent selectivity over GABA-AT, compared with **1** (Table 1). Inactivation pathways for **8** and **9** were elucidated by mass spectrometry and crystallography with the aid of a dialysis experiment, total turnover, and measurement of fluoride ion release. While monofluoro substituted analogue **8** inactivates hOAT via an enamine pathway (Scheme 2, pathway a), difluoro analogue **9** inactivates hOAT via a novel addition-aromatization mechanism (Scheme 2, pathway c), contributing to its significantly enhanced potency. Notably, strikingly accurate masses of intact protein were obtained with errors of less than 1 Da, thereby allowing the facile determination of adduct masses prior to their crystal structures (Table 2). Interestingly, despite the difference in inactivation mechanisms, the turnover mechanisms for **8** and **9** by hOAT are almost identical (Scheme 4, the PLP pathway), and the metabolites were identified with the aid of targeted mass spectrometry. The plausible inactivation and turnover mechanisms for **8** and **9**, supported and rationalized by the use of molecular dynamics (MD) simulations and electrostatic potential (ESP) charge calculations, indicate that a single fluorine atom difference in molecules can control enzyme inactivation mechanisms.

ASSOCIATED CONTENT

Supporting Information

The Supporting Information is available free of charge at <https://pubs.acs.org/doi/10.1021/jacs.0c00193>.

Methods, syntheses, spectra, and crystallographic data (PDF)

AUTHOR INFORMATION

Corresponding Author

Richard B. Silverman — Department of Chemistry, Chemistry of Life Processes Institute, Center for Molecular Innovation and Drug Discovery, and Center for Developmental Therapeutics, Department of Molecular Biosciences, and Department of

Pharmacology, Northwestern University, Evanston, Illinois 60208, United States; orcid.org/0000-0001-9034-1084; Phone: 847-491-5653; Email: Agman@chem.northwestern.edu

Authors

Wei Zhu — Department of Chemistry, Chemistry of Life Processes Institute, Center for Molecular Innovation and Drug Discovery, and Center for Developmental Therapeutics, Northwestern University, Evanston, Illinois 60208, United States; orcid.org/0000-0003-0197-9911

Peter F. Doubleday — Department of Molecular Biosciences, Northwestern University, Evanston, Illinois 60208, United States

Daniel S. Catlin — Department of Chemistry and Biochemistry, Loyola University Chicago, Chicago, Illinois 60660, United States

Pathum M. Weerawarna — Department of Chemistry, Chemistry of Life Processes Institute, Center for Molecular Innovation and Drug Discovery, and Center for Developmental Therapeutics, Northwestern University, Evanston, Illinois 60208, United States

Arseniy Butrin — Department of Chemistry and Biochemistry, Loyola University Chicago, Chicago, Illinois 60660, United States

Sida Shen — Department of Chemistry, Chemistry of Life Processes Institute, Center for Molecular Innovation and Drug Discovery, and Center for Developmental Therapeutics, Northwestern University, Evanston, Illinois 60208, United States; orcid.org/0000-0002-0295-2545

Zdzislaw Wawrzak — Synchrotron Research Center, LS-CAT, Sector 21, Northwestern University, Lemont, Illinois 60439, United States

Neil L. Kelleher — Department of Chemistry, Chemistry of Life Processes Institute, Center for Molecular Innovation and Drug Discovery, and Center for Developmental Therapeutics and Department of Molecular Biosciences, Northwestern University, Evanston, Illinois 60208, United States; orcid.org/0000-0002-8815-3372

Dali Liu — Department of Chemistry and Biochemistry, Loyola University Chicago, Chicago, Illinois 60660, United States; orcid.org/0000-0002-7587-703X

Complete contact information is available at: <https://pubs.acs.org/10.1021/jacs.0c00193>

Notes

The authors declare no competing financial interest.

ACKNOWLEDGMENTS

We are grateful to the National Institutes of Health (grant R01 DA030604 to R.B.S. and grant P30 DA018310 to N.L.K.) and National Science Foundation (grant 2015210477 to P.F.D) for financial support. This work used the Extreme Science and Engineering Discovery Environment (XSEDE) Comet Bridges Stampede2 through allocation TG-CHE190070, which is supported by National Science Foundation grant number ACI-1548562. This work made use of the IMSERC at Northwestern University, which has received support from the Soft and Hybrid Nanotechnology Experimental (SHyNE) Resource (NSF NNCI-1542205), the State of Illinois, and the International Institute for Nanotechnology (IIN). X-ray diffraction data collection used resources of the Advanced Photon Source, a U.S. Department of Energy (DOE) Office of

Science User Facility operated for the DOE Office of Science by Argonne National Laboratory under contract no. DE-AC02-06CH11357. The use of LS-CAT Sector 21 was supported by the Michigan Economic Development Corporation and the Michigan Technology Tri-Corridor (grant 08SP1000817). We thank Dr. Joseph Brunzelle at LS-CAT for help on data collection. We also thank Dr. Matthew J. Moschitto for helpful discussions and Dr. Cory T. Reidl for instruction in molecular docking studies using MOE.

■ ABBREVIATIONS

PMB, *p*-methoxybenzyl; XtalFluor-M, (diethylamino)-difluorosulfonium tetrafluoroborate; Boc, *tert*-butoxycarbonyl; KHMDS, potassium bis(trimethylsilyl)amide; DCM, dichloromethane; DCE, 1,2-dichloroethane; THF, tetrahydrofuran; *m*-CPBA, *m*-chloroperoxybenzoic acid; PCC, pyridinium chlorochromate; Boc₂O, di-*tert*-butyl decarbonate

■ REFERENCES

- (1) Sayiner, M.; Golabi, P.; Younossi, Z. M. Disease Burden of Hepatocellular Carcinoma: A Global Perspective. *Dig. Dis. Sci.* **2019**, *64*, 910–917.
- (2) Personeni, N.; Rimassa, L. Hepatocellular Carcinoma: A Global Disease in Need of Individualized Treatment Strategies. *J. Oncol. Pract.* **2017**, *13*, 368–370.
- (3) Sherman, M.; Bruix, J.; Porayko, M.; Tran, T.; Comm, A. P. G. Screening for hepatocellular carcinoma: The Rationale for the American Association for the Study of Liver Diseases Recommendations. *Hepatology* **2012**, *56*, 793–796.
- (4) Yang, J. D.; Roberts, L. R. Hepatocellular carcinoma: a global view. *Nat. Rev. Gastroenterol. Hepatol.* **2010**, *7*, 448–458.
- (5) Leathers, J. S.; Balderramo, D.; Prieto, J.; Diehl, F.; Gonzalez-Ballera, E.; Ferreira, M. R.; Carrera, E.; Barreyro, F.; Diaz-Ferrer, J.; Singh, D.; Mattos, A. Z.; Carrilho, F.; Debes, J. D. Sorafenib for Treatment of Hepatocellular Carcinoma A Survival Analysis From the South American Liver Research Network. *J. Clin. Gastroenterol.* **2019**, *53*, 464–469.
- (6) de Rosamel, L.; Blanc, J. F. Emerging Tyrosine Kinase Inhibitors for the Treatment of Hepatocellular Carcinoma. *Expert Opin. Emerging Drugs* **2017**, *22*, 175–190.
- (7) Milgrom, D. P.; Maluccio, M. A.; Koniaris, L. G. Management of Hepatocellular Carcinoma (HCC). *Curr. Surg. Rep.* **2016**, *4*, 1–8.
- (8) de Lope, C. R.; Tremosini, S.; Forner, A.; Reig, M.; Bruix, J. Management of HCC. *J. Hepatol.* **2012**, *56*, S75–S87.
- (9) Herzfeld, A.; Knox, W. E. Properties Developmental Formation and Estrogen Induction of Ornithine Aminotransferase in Rat Tissues. *Biochem. J.* **1968**, *243*, 3327–3332.
- (10) Ginguay, A.; Cynober, L.; Curis, E.; Nicolis, I. Ornithine Aminotransferase, an Important Glutamate-Metabolizing Enzyme at the Crossroads of Multiple Metabolic Pathways. *Biology (Basel, Switz.)* **2017**, *6*, 18.
- (11) Zigmund, E.; Ya'acov, A. B.; Lee, H.; Lichtenstein, Y.; Shalev, Z.; Smith, Y.; Zolotarov, L.; Ziv, E.; Kalman, R.; Le, H. V.; Lu, H.; Silverman, R. B.; Ilan, Y. Suppression of Hepatocellular Carcinoma by Inhibition of Overexpressed Ornithine Aminotransferase. *ACS Med. Chem. Lett.* **2015**, *6*, 840–844.
- (12) Herzfeld, A.; Knox, W. E. The Properties, Developmental Formation, and Estrogen Induction of Ornithine Aminotransferase in Rat Tissues. *J. Biol. Chem.* **1968**, *243*, 3327–3332.
- (13) De Ingeniis, J.; Ratnikov, B.; Richardson, A. D.; Scott, D. A.; Aza-Blanc, P.; De, S. K.; Kazanov, M.; Pellicchia, M.; Ronai, Z.; Osterman, A. L.; Smith, J. W. Functional Specialization in Proline Biosynthesis of Melanoma. *PLoS One* **2012**, *7*, e45190.
- (14) Phang, J. M.; Donald, S. P.; Pandhare, J.; Liu, Y. M. The Metabolism of Proline, a Stress Substrate, Modulates Carcinogenic Pathways. *Amino Acids* **2008**, *35*, 681–690.
- (15) Phang, J. M.; Liu, W.; Hancock, C. N.; Fischer, J. W. Proline Metabolism and Cancer: Emerging Links to Glutamine and Collagen. *Curr. Opin. Clin. Nutr. Metab. Care* **2015**, *18*, 71–77.
- (16) Phang, J. M.; Liu, W.; Zabinnyk, O. Proline Metabolism and Microenvironmental Stress. *Annu. Rev. Nutr.* **2010**, *30*, 441–463.
- (17) Phang, J. M.; Liu, W.; Hancock, C.; Christian, K. J. The Proline Regulatory Axis and Cancer. *Front. Oncol.* **2012**, *2*, 60.
- (18) Tang, L.; Zeng, J.; Geng, P. Y.; Fang, C. N.; Wang, Y.; Sun, M. J.; Wang, C. S.; Wang, J.; Yin, P. Y.; Hu, C. X.; Guo, L.; Yu, J. E.; Gao, P.; Li, E. Y.; Zhuang, Z. P.; Xu, G. W.; Liu, Y. Global Metabolic Profiling Identifies a Pivotal Role of Proline and Hydroxyproline Metabolism in Supporting Hypoxic Response in Hepatocellular Carcinoma. *Clin. Cancer Res.* **2018**, *24*, 474–485.
- (19) Heiden, M. G. V.; Cantley, L. C.; Thompson, C. B. Understanding the Warburg Effect: The Metabolic Requirements of Cell Proliferation. *Science* **2009**, *324*, 1029–1033.
- (20) Colnot, S.; Decaens, T.; Niwa-Kawakita, M.; Godard, C.; Hamard, G.; Kahn, A.; Giovannini, M.; Perret, C. Liver-targeted Disruption of Apc in Mice Activates beta-Catenin Signaling and Leads to Hepatocellular Carcinomas. *Proc. Natl. Acad. Sci. U. S. A.* **2004**, *101*, 17216–17221.
- (21) Cadoret, A.; Ovejero, C.; Terris, B.; Souil, E.; Levy, L.; Lamers, W. H.; Kitajewski, J.; Kahn, A.; Perret, C. New Targets of beta-Catenin Signaling in the Liver are Involved in the Glutamine Metabolism. *Oncogene* **2002**, *21*, 8293–8301.
- (22) Liu, Y. F.; Wu, L.; Li, K.; Liu, F. R.; Wang, L.; Zhang, D. L.; Zhou, J.; Ma, X.; Wang, S. Y.; Yang, S. Y. Ornithine Aminotransferase Promoted the Proliferation and Metastasis of Non-small cell Lung Cancer via Upregulation of miR-21. *J. Cell. Physiol.* **2019**, *234*, 12828–12838.
- (23) Markova, M.; Peneff, C.; Hewlins, M. J. E.; Schirmer, T.; John, R. A. Determinants of Substrate Specificity in omega-Amino-transferases. *J. Biol. Chem.* **2005**, *280*, 36409–36416.
- (24) Mehta, P. K.; Hale, T. I.; Christen, P. Aminotransferases - Demonstration of Homology and Division into Evolutionary Subgroups. *Eur. J. Biochem.* **1993**, *214*, 549–561.
- (25) Silverman, R. B. Design and Mechanism of GABA Amino-transferase Inactivators. Treatments for Epilepsies and Addictions. *Chem. Rev.* **2018**, *118*, 4037–4070.
- (26) Silverman, R. B. Mechanism-Based Enzyme Inactivators. *Methods Enzymol.* **1995**, *249*, 240–283.
- (27) Mascarenhas, R.; Le, H. V.; Clevenger, K. D.; Lehrer, H. J.; Ringe, D.; Kelleher, N. L.; Silverman, R. B.; Liu, D. Selective Targeting by a Mechanism-Based Inactivator against Pyridoxal 5'-Phosphate-Dependent Enzymes: Mechanisms of Inactivation and Alternative Turnover. *Biochemistry* **2017**, *56*, 4951–4961.
- (28) Storici, P.; Qiu, J.; Schirmer, T.; Silverman, R. B. Mechanistic crystallography. Mechanism of inactivation of gamma-Aminobutyric Acid Aminotransferase by (1R,3S,4S)-3-Amino-4-fluorocyclopentane-1-carboxylic Acid as Elucidated by Crystallography. *Biochemistry* **2004**, *43*, 14057–14063.
- (29) Juncosa, J. I.; Takaya, K.; Le, H. V.; Moschitto, M. J.; Weerawarna, P. M.; Mascarenhas, R.; Liu, D. L.; Dewey, S. L.; Silverman, R. B. Design and Mechanism of (S)-3-Amino-4-(difluoromethylethyl)cyclopent-1-ene-1-carboxylic Acid, a Highly Potent gamma-Aminobutyric Acid Aminotransferase Inactivator for the Treatment of Addiction. *J. Am. Chem. Soc.* **2018**, *140*, 2151–2164.
- (30) Pan, Y.; Gerasimov, M. R.; Kvist, T.; Wellendorph, P.; Madsen, K. K.; Pera, E.; Lee, H.; Schousboe, A.; Chebib, M.; Brauner-Osborne, H.; Craft, C. M.; Brodie, J. D.; Schiffer, W. K.; Dewey, S. L.; Miller, S. R.; Silverman, R. B. (1S,3S)-3-Amino-4-difluoromethylethyl-1-cyclopentanoic Acid (CPP-115), a Potent gamma-Aminobutyric Acid Aminotransferase Inactivator for the Treatment of Cocaine Addiction. *J. Med. Chem.* **2012**, *55*, 357–366.
- (31) Moschitto, M. J.; Doubleday, P. F.; Catlin, D. S.; Kelleher, N. L.; Liu, D.; Silverman, R. B. Mechanism of Inactivation of Ornithine Aminotransferase by (1S,3S)-3-Amino-4-(hexafluoropropan-2-ylidenyl)cyclopentane-1-carboxylic Acid. *J. Am. Chem. Soc.* **2019**, *141*, 10711–10721.

- (32) Lee, H.; Juncosa, J. I.; Silverman, R. B. Ornithine Aminotransferase versus GABA Aminotransferase: Implications for the Design of New Anticancer Drugs. *Med. Res. Rev.* **2015**, *35*, 286–305.
- (33) Bey, P.; Gerhart, F.; Jung, M. Synthesis of (*E*)-4-Amino-2,5-Hexadienoic Acid and (*E*)-4-Amino-5-Fluoro-2-Pentenoic Acid - Irreversible Inhibitors of 4-Aminobutyrate-2-Oxoglutarate Aminotransferase. *J. Org. Chem.* **1986**, *51*, 2835–2838.
- (34) Wang, Z. Y.; Yuan, H.; Nikolic, D.; Van Breemen, R. B.; Silverman, R. B. (\pm)-(1*S*, 2*R*, 5*S*)-5-amino-2-fluorocyclohex-3-enecarboxylic acid. A Potent GABA Aminotransferase Inactivator that Irreversibly Inhibits via an Elimination-aromatization pathway. *Biochemistry* **2006**, *45*, 14513–14522.
- (35) Jones, G.; Willett, P.; Glen, R. C.; Leach, A. R.; Taylor, R. Development and Validation of a Genetic Algorithm for Flexible Docking. *J. Mol. Biol.* **1997**, *267*, 727–748.
- (36) Qiu, J.; Silverman, R. B. A New Class of Conformationally Rigid Analogues of 4-amino-5-Halopentanoic Acids, Potent Inactivators of gamma-Aminobutyric Acid Aminotransferase. *J. Med. Chem.* **2000**, *43*, 706–720.
- (37) Metro, T. X.; Duthion, B.; Pardo, D. G.; Cossy, J. Rearrangement of beta-Amino Alcohols via Aziridiniums: a review. *Chem. Soc. Rev.* **2010**, *39*, 89–102.
- (38) Wang, X.; Ma, M. L.; Reddy, A. G. K.; Hu, W. H. An Efficient Stereoselective Synthesis of Six Stereoisomers of 3, 4-diaminocyclohexane carboxamide as Key Intermediates for the Synthesis of Factor Xa inhibitors. *Tetrahedron* **2017**, *73*, 1381–1388.
- (39) Beaulieu, F.; Beauregard, L. P.; Courchesne, G.; Couturier, M.; LaFlamme, F.; L'Heureux, A. Aminodifluorosulfonium Tetrafluoroborate Salts as Stable and Crystalline Deoxofluorinating Reagents. *Org. Lett.* **2009**, *11*, 5050–5053.
- (40) Pan, Y.; Qiu, J.; Silverman, R. B. Design, Synthesis, and Biological Activity of a Difluoro-substituted, Conformationally Rigid Vigabatrin Analogue as a Potent gamma-Aminobutyric Acid Aminotransferase Inhibitor. *J. Med. Chem.* **2003**, *46*, 5292–5293.
- (41) Lee, H.; Doud, E. H.; Wu, R.; Sanishvili, R.; Juncosa, J. I.; Liu, D. L.; Kelleher, N. L.; Silverman, R. B. Mechanism of Inactivation of gamma-Aminobutyric Acid Aminotransferase by (1*S*,3*S*)-3-Amino-4-difluoromethylene-1-cyclopentanoic Acid (CPP-115). *J. Am. Chem. Soc.* **2015**, *137*, 2628–2640.
- (42) Liebschner, D.; Afonine, P. V.; Moriarty, N. W.; Poon, B. K.; Sobolev, O. V.; Terwilliger, T. C.; Adams, P. D. Polder Maps: Improving OMIT Maps by Excluding Bulk Solvent. *Acta. Crystallogr. D* **2017**, *73*, 148–157.
- (43) Egli, M.; Sarkhel, S. Lone pair-aromatic Interactions: To Stabilize or not to Stabilize. *Acc. Chem. Res.* **2007**, *40*, 197–205.
- (44) Montioli, R.; Paiardini, A.; Giardina, G.; Zanzoni, S.; Cutruzzola, F.; Cellini, B.; Voltattorni, C. B. R180T Variant of delta-Ornithine Aminotransferase Associated with Gyrate Atrophy: Biochemical, Computational, X-ray and NMR Studies Provide Insight into its Catalytic Features. *FEBS J.* **2019**, *286*, 2787–2798.
- (45) Storici, P.; Capitani, G.; Muller, R.; Schirmer, T.; Jansonius, J. N. Crystal Structure of Human Ornithine Aminotransferase Complexed with the Highly Specific and Potent Inhibitor 5-Fluoromethylornithine. *J. Mol. Biol.* **1999**, *285*, 297–309.
- (46) Faraci, W. S.; Walsh, C. T. Mechanism of Inactivation of Alanine Racemase by β , β -Trifluoroalanine. *Biochemistry* **1989**, *28*, 431–437.